Research Article Vol. 33, No. 12 / 16 Jun 2025 / Optics Express 25693
Optics EXPRESS

Single-beam and -detector laser-absorption velocimetry, non-equilibrium thermometry, and nitric oxide measurements at near-MHz rates in hypersonic air

JONATHAN J. GILVEY,[1,*] ELIJAH R. JANS,[2] CHARLEY R. DOWNING,[2] BRADLEY T. LYON,[2] KYLE P. LYNCH,[2] JUSTIN L. WAGNER,[2] AND CHRISTOPHER S. GOLDENSTEIN[1]

[1]School of Mechanical Engineering, Purdue University, 585 Purdue Mall, West Lafayette, IN 47907, USA
[2]Sandia National Laboratories, Albuquerque, NM 87123, USA
[*]jgilvey@purdue.edu

Abstract: This manuscript presents a quantum-cascade-laser-absorption-spectroscopy (QCLAS) diagnostic for measuring the rotational and vibrational temperatures, partial pressure, and velocity of nitric oxide (NO) in hypersonic flows at rates up to 500 kHz. Two fiber-coupled distributed-feedback QCLs and a 3D-printed optical probe were used to measure the aforementioned properties via a single retroreflected beam and a single detector. This approach was taken to minimize spatial averaging and sensor complexity while still providing a self-referenced calibration-free velocity measurement. Two 3D-printed optical probe designs are presented, and design guidelines for minimally invasive probes in hypersonic test facilities are discussed. The diagnostic was applied in the freestream of a reflected-shock tunnel for flow enthalpies of 3.8, 10.3, and 12 MJ/kg, which correspond to velocities near 3, 4, and 5 km/s. The quasi-steady flow conditions were characterized and compared to CFD predictions. In general, the measured quantities agreed relatively well with CFD predictions except for the vibrational temperature of NO and the observation of some high-frequency oscillations in freestream conditions. The high measurement rate of the diagnostic was critical to quantifying the latter.

1. Introduction

Many hypersonic ground-test facilities (HGTFs) generate flows that are characterized by a large degree of chemical and thermal non-equilibrium. This is because HGTFs often utilize a reservoir containing a gas at high-temperature and -pressure which is expanded through a nozzle to high Mach numbers. The translational temperature and densities both drop rapidly during the expansion of the gas through the nozzle. This may result in the internal energy modes of the molecules not reaching a state of thermal equilibrium defined by a single temperature. Additionally, species which are formed at high temperatures (e.g., NO and O) may be frozen in the flow. Researchers need to quantify the thermochemical state of the gas in the freestream to understand the state of the gas, accurately model gas-surface chemistry, and to confirm the accuracy of CFD simulations. Quantifying the non-equilibrium flow in HGTFs is important as it can impact the freestream velocity, post-shock gas conditions, shock geometries, the forces acting on experimental models, shock-boundary layer interaction, and flow transition to turbulence [1–3].

Impulse-type HGTFs, such as reflected-shock tunnels, generate flows characterized by a significant degree of thermochemical non-equilibrium in their freestream. One technique used to make measurements in HGTFs is laser absorption spectroscopy (LAS) which is particularly attractive due to its non-intrusive nature, ability to provide quantitative and calibration-free

#560378 https://doi.org/10.1364/OE.560378
Journal © 2025 Received 25 Feb 2025; revised 28 Apr 2025; accepted 29 Apr 2025; published 9 Jun 2025

Optics EXPRESS

measurements of multiple flow properties simultaneously, its relative simplicity, low cost, and its ability to provide high-speed (>100 kHz) measurements. Over the past thirty years several works have been published detailing the utilization of LAS for characterizing thermal non-equilibrium and velocity in impulse-type HGTFs. Several relevant and notable bodies of work will now be discussed in chronological order. Wehe et al. measured H_2O and potassium (K) at 10 kHz and extracted measurements of velocity, translational and rotational temperatures, and H_2O partial pressure in the CUBRC LENS tunnel [4,5]. Mohamed et al. made measurements of NO, CO, and H_2O velocities and translational temperatures in the F4, HEG, and S4MA tunnels at rates up to 20 kHz using lead-salt diode lasers [6]. Seven years later Parker et al. reported on 1 kHz measurements of NO translational and rotational temperatures and concentration [7], and 10 kHz measurements of velocity [8] in the CURBC LENS facility using a quantum cascade laser (QCL). The Doppler shifts used for velocity measurements in Wehe et al., Mohamed et al. and Parker et al. were calibrated using a reference static cell. In another approach, Meyers et al., measured CO_2 translational temperatures and velocity in the Von Karman Institute's (VKI) Longshot tunnel using an external cavity diode laser near 1.6 μm [9]. The researchers used a single beam where the beam was passed once downstream then redirected to the opposite side of the freestream through a rigid tube. The beam was then directed upstream through the flow and the light was measured on a detector which allowed for single-detector velocimetry via multiple lines of sight and measurement locations. In the early 2020s Girard et al. and Finch et al. made 50 kHz measurements of NO rotational and vibrational temperatures, number densities, and velocities in Caltech's T5 tunnel. The group also measured CO, H_2O, and K present in the flow without directly seeding any of the aforementioned species into the test gas [10,11]. The measurement of CO and H_2O is notable, since these species likely resulted from contamination within the facility. Further, water is of particular interest for freestream characterization as it increases vibrational relaxation rates of diatomics dramatically [12]. Similar diagnostics by the same research group have also been applied to near-body flows in the T5 [13].

Recently, a collaborative effort between our group and Sandia National Laboratories (SNL) has focused on providing a highly detailed characterization of the freestream of SNL's Hypersonic Shock Tunnel (HST) using several laser diagnostics. Jans et al. made coherent anti-Stokes Raman scattering (CARS) measurements of the rotational and vibrational temperatures of the non-IR active species N_2 and O_2 at 100 kHz [14]. Molecular-tagging velocimetry (MTV) measurements of NO at 50 kHz were also acquired [14]. Our research group made LAS measurements of the rotational and vibrational temperatures and partial pressure of NO, and H_2O partial pressure in the freestream of the HST at 25 kHz or 100 kHz, depending on the flow conditions [15]. Together, these works detail a coordinated effort to fully characterize the freestream rotational and vibrational temperatures, NO and H_2O partial pressures, and velocity in hypersonic flows produced by the HST. Notably, experiments using >3000 ppm of water did not show discernible differences in vibrational relaxation of NO compared to tests with dry air.

While not a complete list, the following notable works deal with LAS measurements using hardened probes which are relevant to this work. Wehe et al. used a probe similar to the first probe used in this work. They observed absorbance from within the probe and from viscous flow within the boundary layer [4,5]. Vallon et al. used a probe to make LAS measurements in the VKI Longshot tunnel and the ONERA F4 wind tunnel [16]. Schlieren images of the probe revealed oblique shocks emanating from the leading edges. However, the shocks were weak and their impact on the velocity is expected to be less than 10%. Xu et al. measured the velocity of H_2O at 5 kHz in a pulsed-combustion wind tunnel at the China Aerodynamic Research and Development Center [17]. Their diagnostic consisted of four velocity probes placed near the exit of the nozzle and spaced transverse to the flow. Schlieren imaging of the probes showed no significant shocks between the flow diverters. This was surprising as the flow exiting the nozzle is expected to be conical and thus should be turned by minor shocks.

Optics EXPRESS

Schwartz et al. used fixed flow cutters to isolate the hypersonic core flow in the California Institute of Technology's Hypervelocity Expansion Tube and acquired 200 kHz measurements of the translational temperature and velocity of K [18]. In another work, Schwartz et al. used a fixed probe in the Stanford Flexible Application Shock Tube to make 200 kHz measurements of velocity by targeting K [19]. The probe's internal faces were angled outwards by 1° to prevent the formation of oblique shocks between the probe's arms. Additionally, a multimode fiber was used to catch the laser light, although this introduced noise into the absorption signal.

Single-beam velocimetry requires either a frequency-stabilized source, a reference gas cell for wavelength calibration, or opposing Doppler shifts. A recent example of the first technique is that used by Yun et al. where a frequency-stabilized dual-frequency comb was used to make single-beam, single LOS velocimetry measurements [20]. However, these measurements were acquired at 625 Hz over a broad spectral region in the near-IR for H_2O. The flow durations in shock tunnels are on the order of hundreds of microseconds and a much faster measurement rate is needed. Examples of the second technique can be found in many of the sources already mentioned. Finally, an example of the third technique can be found in Kurtz et al. who developed a single-beam multi-path LAS diagnostic for the inlet of a scramjet to measure oxygen at 40 Hz [21,22]. Meyers et al. also used a single beam, albeit without retroreflecting the beam and instead used additional hardware to perform crossed-beam velocimetry [9].

This work describes an LAS diagnostic for measuring the rotational and vibrational temperatures, partial pressure, and velocity of NO at 100 or 500 kHz depending on the flow conditions. The primary novelty of this work is threefold. (1) To the authors' knowledge, this work presents the fastest velocimetry rate ever acquired using LAS and the fastest simultaneous measurements of non-equilibrium thermometry, partial pressure, and velocimetry. (2) The diagnostic provides self-referenced and calibration-free velocity measurements using a single retroreflected beam that was minimally offset in space. To the authors' knowledge, this is the first implementation of quasi-single-LOS, single-beam, and single-detector LAS velocimetry in a hypersonic flow. This approach offers several important advantages, namely: more sensitive and accurate velocimetry due to doubling the Doppler shift and being self-referenced, and reduced spatial averaging through the flow. (3) The diagnostic uses a minimally invasive 3D-printed optical probe that was tailored to the flow geometry. Several important design recommendations, that are informed by previous probe designs, are presented to avoid significant disturbance of the freestream. Lastly, in this work, measurements were acquired at flow enthalpies of 3.8, 10.3, and 12.0 MJ/kg. These enthalpies correspond to targeted freestream velocities of 3, 4, and 5 km/s, respectively. However, in the HST these velocities were unable to be achieved due to non-ideal effects. As a result, throughout this paper, the test conditions are referred to as low, medium, and high enthalpy.

2. Theory

2.1. Laser absorption spectroscopy

In LAS laser light is measured on a detector whose output is linearly proportional to the light intensity. In QCLAS a QCL is fed a modulated current waveform that simultaneously modulates the laser's intensity and wavelength. The laser intensity at optical frequency $\widetilde{\nu}$ (cm^{-1}) is measured in the absence of an absorbing medium ($I_0(\widetilde{\nu})$) and with an absorbing medium present ($I_t(\widetilde{\nu})$). The absorbance of the medium $\alpha(\widetilde{\nu})$ can then be calculated using the Beer-Lambert law: $\alpha(\widetilde{\nu}) = -\ln\left(\frac{I_t(\widetilde{\nu})}{I_0(\widetilde{\nu})}\right)$.

For an ideal diatomic gas in thermal non-equilibrium, the absorbance $\alpha(\widetilde{\nu})$ measured over a path length of L (cm) is given in Eq. (1). Here, $S_{i,j}(T_{tr,rot}, T_{vib})$ (cm^{-2}/atm) is the linestrength of transition j for absorbing species i at translational/rotational temperature $T_{tr,rot}$ (K) (assumed to be equal) and vibrational temperature T_{vib} (K), P (atm) is the pressure, χ_i is the mole fraction of the absorbing species i, $\phi_{i,j}(\widetilde{\nu})$ is the lineshape (cm), and dL (cm) is the differential path length.

Optics EXPRESS

The non-equilibrium model used in this work is discussed in detail by Gilvey et al. [15] and for brevity is not presented here.

$$\alpha(\widetilde{\nu}) = \int_0^L \sum_{i,j} S_{i,j}(T_{tr,rot}, T_{vib}) P \chi_i \phi_{i,j}(\widetilde{\nu})\, dL \tag{1}$$

In this work the Doppler full-width at half-maximum (FWHM) is expected to be much larger than the collisional broadening FWHM due to the low pressures in the freestream of the HST (≈0.005 atm). Also, the Doppler shift is expected to be approximately three times larger than the Doppler FWHM of the transitions. This results in relatively large separation of the transitions and thus, accurate measurements of the Doppler shift. The Doppler broadening FWHM of the transitions is over 25 times greater than the transit-time FWHM [23]. As a result, the dominant broadening mechanisms are Doppler and collisional broadening, which are both accounted for by the Voigt profile. Lastly, the measured absorbance spectra are slightly instrument broadened due to the response time of the detector and the high chirp rate of the QCLs. The impact of this instrument broadening was investigated via absorbance simulations with Gaussian instrument broadening near 0.001 cm^{-1} (dictated by the known laser chirp rate and detector response time). Instrument broadened spectra were post-processed with the same spectral-fitting routine used to analyze measured spectra, and the impact of instrument broadening upon the measured thermodynamic properties was found to be negligible compared to the measurement uncertainties. This topic is discussed in greater detail in the Supplemental Material document.

Absorption transitions are Doppler shifted if the gas is moving along the direction of laser light propagation with non-zero velocity. The equation for the Doppler shift $\delta\widetilde{\nu}$ (cm^{-1}) is: $\delta\widetilde{\nu} = \widetilde{\nu}_0 \frac{u_{||}}{c}$. Here $\widetilde{\nu}_0$ (cm^{-1}) is the transition wavenumber in the absence of gas movement, $u_{||}$ (cm/s) is the projected gas velocity along the direction of light propagation, and c (cm/s) is the speed of light.

3. Sensor design and operation

3.1. Line selection

The transitions used in this study were used in our previous work [15] which used a lower measurement rate and an entirely different probe design. In that work the internal temperatures and partial pressures of NO were measured but velocity was not. Figure 1 (top) shows the absorbance spectrum for the fundamental vibration bands of NO in thermal non-equilibrium at $T_{tr,rot}$ = 194 K, T_{vib} = 781 K , P = 507 Pa (0.005 atm), χ_{NO} = 0.026%, and L = 30.5 cm (12"). The spectra correspond to a low-enthalpy test with no Doppler shift and for a LOS near the nozzle exit plane. Figure 1 (bottom) shows the transitions targeted by QCL1 (left) and QCL2 (right) with the expected Doppler shifts for a velocity of 3 km/s. The spectra of the upstream propagating and downstream propagating beams are shown separately for clarity. In the bottom plots the absorbance spectra for CO and H_2O at mole fractions of 1% are negligible. These species were not expected in large quantities (>1% mole fraction), however, contamination in reflected shock-tunnel facilities has been observed by others [10,11]. Four transitions in the fundamental vibration bands of NO were used in this study. For low-enthalpy tests the R(0,2.5), R(0,16.5), R(1,11.5) transitions in the $X^2\Pi_{3/2}$ electronic state and the R(0,2.5) transition in the $X^2\Pi_{1/2}$ electronic state were measured. For medium- and high-enthalpy tests the R(0,2.5) transition in the $X^2\Pi_{3/2}$ electronic state was not included as the absorbance signal was too weak due to low laser power which resulted from the limited scan depth of QCL1 at high scan frequencies. The notation R(v'', J'') denotes a R-branch transition of NO from a lower state with vibrational and rotational quantum numbers v'' and J'', respectively. The temperature sensitivities of the chosen transitions are all above one for the conditions studied and are discussed in Gilvey et al. [15]. For clarity, the mode-specific temperature sensitivity is given by: $\frac{dR/R}{dT_i/T_i} = \left(\frac{hc}{k_B}\right) \frac{E''_{2,i} - E''_{1,i}}{T}$

Optics EXPRESS

(K^{-1}). Here, R is the ratio of linestrengths for the two transitions used for thermometry, T_i is the mode-specific temperature (e.g., rotational), and $E''_{2,i} - E''_{1,i}$ is the maximum difference in mode-specific lower-state energies for the transitions used for thermometry.

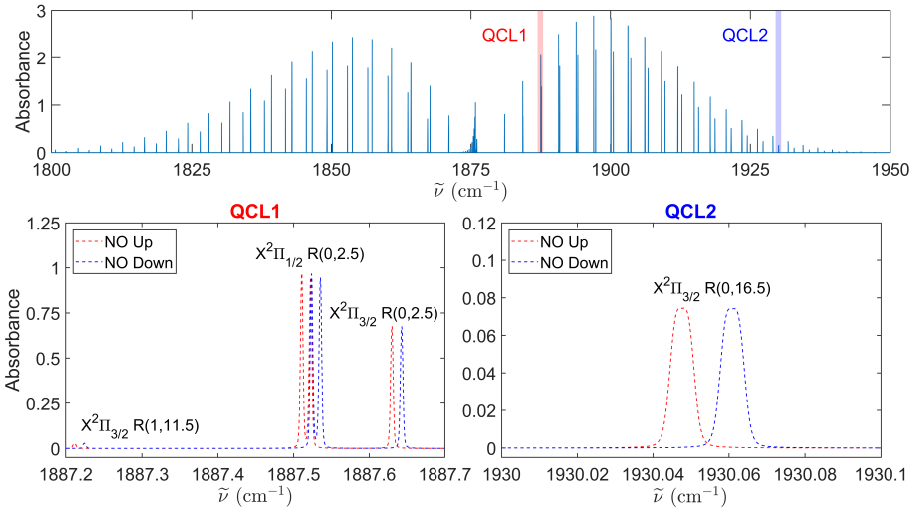

Fig. 1. (Top) Non-equilibrium absorbance of NO at rest. (Bottom) Doppler-shifted spectra for QCL1 (left) and QCL2 (right). The spectra are for low-enthalpy using a 70° crossing angle. Absorbance from CO and H_2O at mole fractions of 1% is negligible.

3.2. Optical hardware and probe design

3.2.1. Laser fiber coupling and electronics

Figure 2 shows a schematic of optics used for fiber coupling the QCLs. Two QCLs were both fiber-coupled into a single-mode InF_3 fiber using a 5-axis fiber-coupling mount (ThorLabs FiberPort). Prior to entering the FiberPort the light from the QCLs passed through ZnSe plano-convex (PC) lenses which increased the fiber-coupling efficiency by 300%. An optical isolator placed before the FiberPort attenuated back reflections and reduced noise. The DC current and temperature control of the lasers was provided by two QCL 6310 laser controllers (Arroyo Instruments). The DC currents of the laser controllers were combined with an RF signal from arbitrary function generators (AFGs) using two bias-tees. The RF+DC signal was sent to both of the lasers to tune the current and wavelength of the lasers. The lasers were time-multiplexed so that only one laser was on at a time. The laser light was measured on a high-speed detector (500 MHz bandwidth) and an oscilloscope with a bandwidth of 1 GHz sampled the detector signal at 6.25 GS/s. The AFGs scanned the lasers at 100 kHz for low-enthalpy tests and 500 kHz for medium- and high-enthalpy tests. More details on the specific equipment can be found in Gilvey et al. [15].

3.2.2. Optical probe design details

Accurately measuring the internal temperatures, species partial pressures, and velocity in hypersonic flows requires that the diagnostic does not significantly disturb the flow. As LAS is a path-integrated technique, it is also desirable to measure only the region of the flow which has quasi-uniform properties. As a result, non-uniform regions (e.g., boundary layers) should be reduced and avoided as much as possible along the laser's LOS. In this work, two probes using flow cutters were used to isolate the quasi-uniform core flow of the HST. Our experience with these and our original probe design [15] has led to the following design recommendations. The flow cutters should have the following features: (1) sharp leading edges to not introduce shocks

Optics EXPRESS

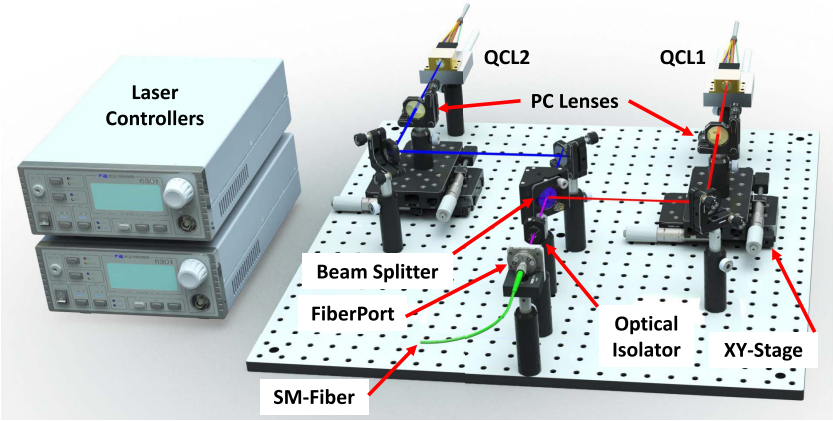

Fig. 2. Schematic of the setup for coupling two QCLs into a single mode fiber.

at the leading edges. Razor blades were used here. (2) Angled faces which are shallow so as not to introduce significant shocks. (3) LOS-facing surfaces which are aligned with the flow and slightly expanded so as not to introduce an oblique shock. (4) A design which isolates the absorbing path to only the quasi-uniform flow. (5) Last, beams which are located close to the leading edge of the flow cutters to reduce the impact of shocks and boundary layers that grow along the probe. Regarding item 3, weak shocks on faces aligned with the flow may be inevitable due to viscous interaction which increases with Mach number [24].

In this study, the center of the LOS for both probes was spaced 7 cm from the HST nozzle exit plane. The first probe (hereon referred to as probe 1) and the second probe (hereon referred to as probe 2) were 3D-printed on a Form 3L and Form 4 3D-printer (FormLabs) using rigid 10K resin (FormLabs). Figure 3 shows renderings of probe 1 (left) and probe 2 (right) at the same scale. The nozzle of the HST can be seen at the top of the images. Both probes had lids which sealed the internal volume at atmospheric pressure and these have been hidden.

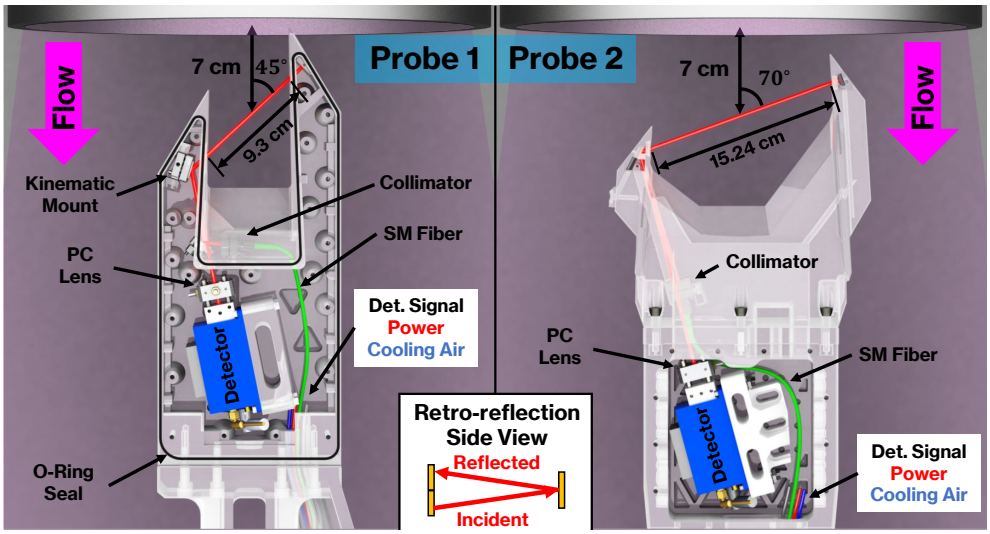

Fig. 3. Renderings of probe 1 (left) and probe 2 (right) in the HST at the same scale.

Optics EXPRESS

Both probes utilized a fiber collimator (ThorLabs F028APC-4950), mirrors, and a high-bandwidth AC-coupled detector (VIGO Photonics FIP-1k-1G-ND) that were placed inside of the probe bodies. The probe bodies were maintained at atmospheric pressure and sealed from the test section. The detector was placed directly in the probe bodies to avoid the use of a multimode catch fiber. A single-mode (SM) InF_3 fiber (ThorLabs P3-32F-FC-2), a power cable for the detector, SMA cable for the detector signal, and an air-cooling line were fed in to the probe body using a baffled vacuum hose with KF25 fittings. Cooling air for the detector was fed in at approximately 1 CFM and was able to exit the probe though the empty space in the vacuum hose. For both probes the laser beam was pitched from the collimator and directed out of a thin CaF_2 window (Probe 1: Ø=2.54 cm, Probe 2: Ø=1.27 cm). The beam then propagated upstream and a mirror on the other side of the probe retroreflected the beam. The pitch and reflected beams were angled into the page to separate the beams and prevent interference fringes. This is indicated schematically at the center-bottom of Fig. 3. The reflected beam was directed with a separate mirror on the catch side towards the detector. An AR-coated ZnSe PC lens (Thorlabs LA7477-E2) with a focal length of 15 mm focused the laser light onto the detector's active area. The windows on both probes were affixed to the probe and made airtight using a quick-setting epoxy.

This paragraph discusses design aspects that are unique to probe 1. Probe 1 had leading edges that consisted of the 3D-printed material. The internal-facing planar faces were expanded by 1° relative to the central axis of the flow so as to not introduce an oblique shock. However, CFD simulations of the HST predict that the flow would be turned inward by 0.32° (due to the expanding conical flow). The laser beams were located approximately 5.3 cm and 3.8 cm from the leading edges on the pitch and the reflected sides, respectively. The single-direction path length of the laser beam was nominally 9.25 cm and the angle of the beam relative to the flow was nominally 45°. Kinematic mounts (Thorlabs Mini-Series) were used to articulate the mirrors and direct the beam. A large O-ring and sealing pan head screws were used to seal the internal volume, however, a small amount of room-temperature vulcanizing silicone (RTV Permatex 82180) still needed to be applied to form an airtight seal. Lastly, the leading edges measure 7.62 cm into the page.

This paragraph discusses design aspects that are unique to probe 2. Probe 2 had razor blades placed at the leading edges of the flow cutters to reduce any minor shock that could form from a blunted leading edge. The planar faces holding windows were expanded by 0.5° relative to the streamlines of the flow (predicted from CFD) which introduced a very small expansion region. The laser beams were located approximately 1.8 cm and 2.3 cm from the leading edges on the pitch and the reflected sides, respectively. The single-direction path length of the laser beam was nominally 15.24 cm and the angle of the beam relative to the flow was nominally 70°. Shimmed mirrors were used to direct the beam. The mirrors were cut from a 2 mm thick protected silver mirror (ThorLabs PFR14-P02). Aluminum shims with adhesive backing were placed between the mirrors and their stops to allow for precise articulation of the mirrors. Only RTV was used to form an airtight seal of the internal volume and the leading edges measure 1.9 cm into the page.

Probe 2 was developed after using probe 1 in the HST and several design improvements that probe 2 has are discussed here. First, the internal-facing planar faces of probe 2 are expanded by 0.5° relative to the flow to introduce a very minor expansion region and avoid generating minor shocks. Second, the beams were spaced closer to the leading edges of the flow cutters. This was accomplished by using shimmed mirrors instead of mirrors in kinematic mounts. Third, the path length was increased to improve signal levels. Fourth, razor blades were added to the flow cutter leading edges to precisely separate the flow. Fifth, the beam angle relative to the flow was increased to 70° to reduce the impact of varying flow properties along the laser's LOS (due to the expanding flow). However, the impact of non-uniformities along the LOS was minor and is detailed in the supplementary material. Sixth, the large O-ring groove between the probe body

Optics EXPRESS

and lid was removed and the seal was formed with RTV. Last, the probe body and the body with the flow cutters were separate parts that were affixed with screws and sealed with RTV. The main benefit is that the body with the leading edges can be easily replaced at low cost. The modular design allows for modification and use at other locations in the HST or in different facilities.

The path length and angle of the laser beams must be known in order to make accurate partial pressure and velocity measurements. This was performed by referencing images of the windows and the laser beam spot on a detector card. An example of characterizing the laser beam alignment is given in the supplementary material.

4. Sandia HST

The Sandia HST is a free-piston reflected-shock tunnel located at Sandia National Laboratories. The shock tube portion of the tunnel consists of a free-piston driver which near isentropically compresses a driver gas to high-pressure and -temperature. Upon rupturing a steel diaphragm a shock wave propagates into the driven region which contains the test gas. The shock reflects off the endwall and then propagates back into the already shocked gas and heats and compresses the gas to even higher temperature and pressure. Located at the endwall is a small entrance to the nozzle which is initially isolated from the test gas by a thin Mylar diaphragm that is ruptured after the shock reflects off the endwall. During the start-up a shockwave passes through the nozzle and into the test section and there is a short period of transient flow. After this the shock tunnel reaches its quasi-steady operating point. More details of the HST can be found in Lynch et al. [25] and Jans et al. [14]. In this work the driver gas was either helium or a mixture of helium and argon and the driven gas was a bottled mixture of 80% nitrogen and 20% oxygen. For all tests, the trigger (time zero) came from a pressure transducer located in the stagnation chamber of the HST. Pitot pressure measurements were acquired during the test time without the flow cutters present. This was accomplished by using a rake instrumented with 17 alternating PCB sensors (PCB 113B27 and 113B28). The rake was located 23 cm downstream of the nozzle exit plane and the sensors were sampled at 2 MS/s [14]. MTV measurements are also included here for comparison [14]. Lastly, details of the MTV measurements and CFD simulations for the HST can be found in the supplementary material.

5. Results

5.1. High-speed video stills and best-fit absorbance spectra

Figure 4 shows still images of probe 1 (left) and probe 2 (right) from a high-speed video of a high-enthalpy test. The still images correspond to 560 μs and 572 μs after the trigger for probe 1 and probe 2, respectively. Also shown in red are the approximate beam locations for both probes. Disturbances to the flow can be seen aft the leading edges of probe 1 (i.e., the shadows on the probe body). The approximate angle of this disturbance (assumed to be an oblique shock) is 12.57° on the pitch side and 11.33° on the reflected side. For probe 2, no disturbance to the flow can be seen. From the images, and later shown in LAS measurements, it is expected that the disturbance visible in probe 1 leads to a slightly higher rotational temperature, a slightly lower velocity, and an increased NO partial pressure. The probe 1 disturbance is expected to come from a combination of a slight turning of the flow, viscous interaction, and minor shocks at the leading edges. In contrast, results obtained using probe 2 are less impacted by flow disturbances.

Figure 5 (top) shows the measured detector signal of I_t (red) and I_0 (black) for a single scan of both lasers vs. time. The trace is for a low-enthalpy test using probe 2. Figure 5 (middle) shows the measured (black dots) and best-fit (dashed red) absorbance spectra vs. relative wavenumber for QCL1 (left) and QCL2 (right). Figure 5 (bottom) shows the peak-normalized residuals for the absorbance plots. The measured spectra are a sum of the upstream and downstream absorbance where the upstream spectrum is red shifted and the downstream spectrum is blue shifted. The

Optics EXPRESS

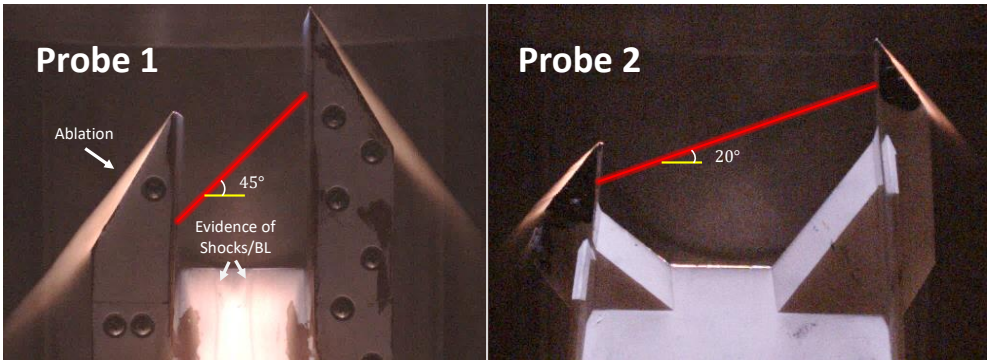

Fig. 4. Still images from high-speed videos of probe 1 (left) and probe 2 (right). The images are for a high-enthalpy test and correspond to the quasi-steady time at ≈565 μs.

residuals for the R(0,2.5) transitions are primarily below 5%. Their shape and amplitude result from a combination of the high characteristic frequency of the transitions [26] (near the detector bandwidth) and the high signal-to-noise ratio. The integrated absorbance and shape of the transitions will be altered if the characteristic frequency of the transitions is near the detector bandwidth. Care was taken as to not have the bandwidth limitation of the detector introduce significant error into the measured absorbance [15]. The residuals for the R(1,11.5) transition

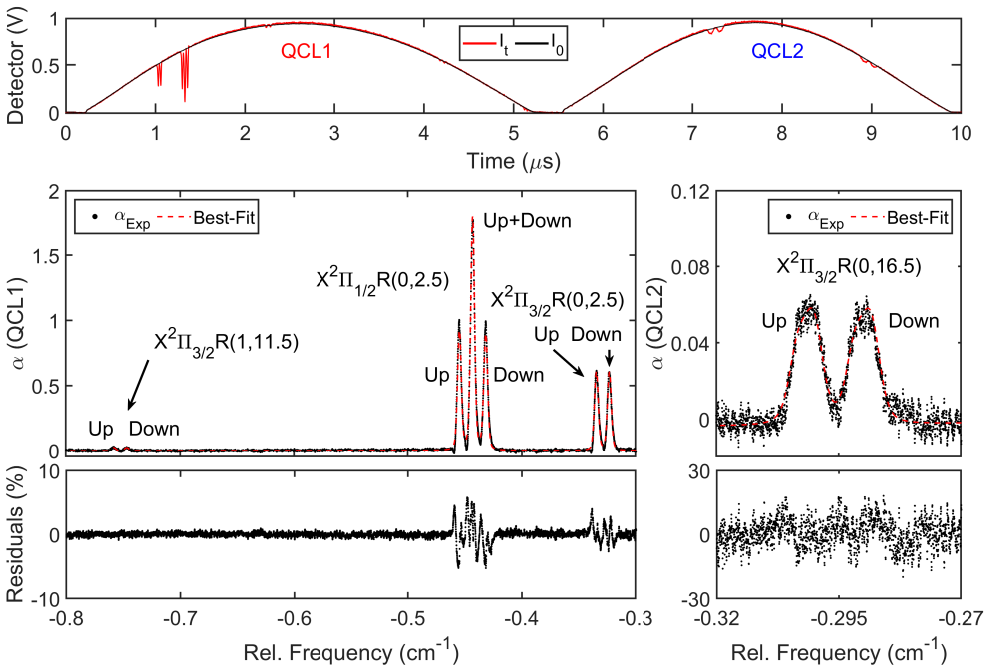

Fig. 5. (Top) I_t (red) and I_0 (black) for a single scan of both lasers vs. time. (Middle) Measured (black dots) and best-fit (dashed red) absorbance vs. relative wavenumber for QCL1 (left) and QCL2 (right). (Bottom) Peak-normalized residuals.

are buried in the noise floor of the measurement. The max residuals for the R(0,16.5) transition are near 20% due to the relatively low absorbance. However, there are a sufficient number of data points such that any noise is effectively filtered by the fitting routine. The spectra shown

Optics EXPRESS

correspond to 1271 μs after the trigger with best-fit parameters of 183 K, 762 K, 11.1 Pa, and 2640 m/s for $T_{tr,rot}$, T_{vib}, P_{NO}, and velocity, respectively.

5.2. $T_{tr,rot}$, T_{vib}, P_{NO}, and velocity measurements

Section 5.2.1 presents LAS measurements for low-enthalpy tests using probe 1 and probe 2. For the test cases of medium and high enthalpy only the probe 2 data is shown. The probe 1 measurements are not shown in the later sections since probe 1 is shown to disturb the flow significantly. For all tests shown in the following sections, the shaded regions on the probe 1 LAS traces corresponds to the min and max values measured across three separate tests. This was done to highlight the shot-to-shot repeatability of the tunnel. The shaded regions on the probe 2 LAS measurements correspond to the 95% confidence intervals (CIs) on the fit parameters which were returned from the fitting routine. This was done to highlight the low uncertainty of the best-fit parameters returned from the fitting routine. The shaded regions on the MTV measurements are the standard error for 10, five, and three tests for low-, medium-, and high-enthalpy tests, respectively. The shaded regions on the pitot pressure measurements are the standard error for 22, eight, and six tests for low-, medium-, and high-enthalpy tests, respectively. In the CFD simulations, two sets of rates for the vibrational relaxation time of NO were used. The "Park" model used vibration-translation (VT) relaxation rates from Park [27] and vibration-vibration (VV) relaxation rates from Kim et al. ([28]). The Streicher model used VT and VV rates for NO-N_2 and NO-NO from Streicher et al. [29,30]. All VV rate correlations were least-squares fit to the empirical model described in Kearney et al. [31]. The measurements from LAS and the predictions from CFD are shown in Table 1.

Table 1. Quasi-steady values averaged between 1121 μs and 1691 μs (low-enthalpy test) and between 486 μs and 694 μs (high-enthalpy test). The LAS standard deviation is in parentheses. CFD predictions from fitting to simulated path-integrated absorbance spectra are also included.

	3.80 MJ/kg enthalpy			12.0 MJ/kg enthalpy		
		CFD			CFD	
Parameter	Probe 2 LAS	Park	Streicher	Probe 2 LAS	Park	Streicher
T_{vib} (K)	812 (19.0)	378	547	707 (85.3)	802	996
$T_{tr,rot}$ (K)	186 (2.1)	188	188	579 (25.7)	664	663
u (m/s)	2660 (24)	2660	2660	4210 (59.2)	4540	4540
P_{NO} (Pa)	11.1 (0.577)	9.97	10.0	20.3 (1.38)	13.6	13.6

5.2.1. LAS measurements at low enthalpy using two probes

Figure 6 shows a time history of measured LAS values for a low-enthalpy test using probe 1 (red) and probe 2 (black). Included in the figure are the vibrational temperature (A), rotational temperature (B), velocity (C), NO partial pressure (D, left axis), and pitot pressure (D, right axis). The LAS velocity measurements are complimented by MTV measurements (blue). Also shown are CFD predictions using the Park (dashed black) and Streicher (dashed blue) rates for NO vibrational relaxation. The 95% CI bands for probe 2 in B, C, and D are too small to be seen. The quasi-steady test time appears to be between 1121 μs and 1691 μs. The quasi-steady test time was taken as the point where the rotational temperature has plateaued, the velocity is quasi-constant, and where P_{NO} is relatively constant. Table 1 tabulates the measured LAS properties for probe 2 during this quasi-steady test time. The standard deviations of the measurements during this time are shown in the parentheses. Also shown in this table are predicted measurements from CFD which were determined by fitting to path-integrated synthetic spectra. The fitting of synthetic spectra is described in the supplementary material. The different vibrational relaxation models

Optics EXPRESS

primarily impact the predicted NO vibrational temperatures while $T_{tr,rot}$, P_{NO}, and the velocity remain relatively unaffected. Additionally, when using the same rate model, there are only minor differences between the two probe's lines-of-sight.

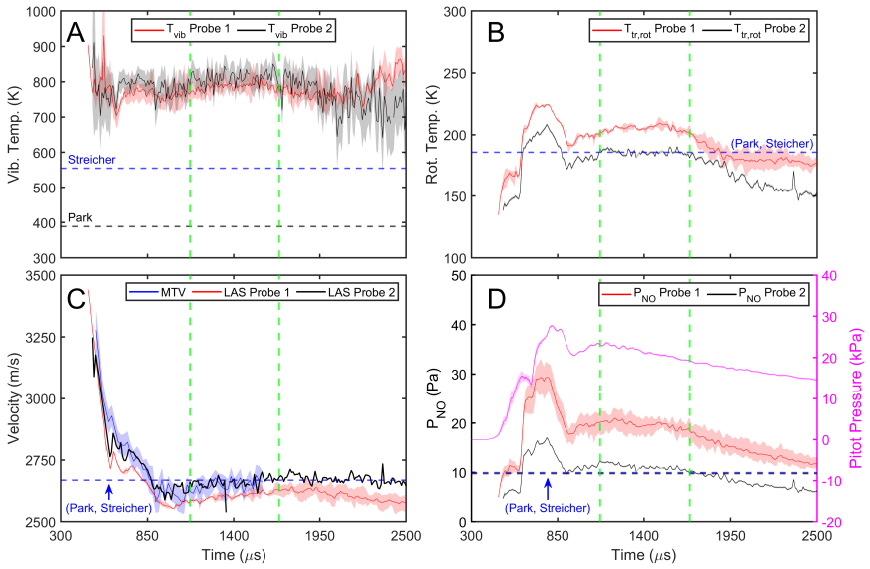

Fig. 6. (A) Measured T_{vib}, (B) $T_{tr,rot}$, (C) velocity by MTV (blue) [14] and the two probes in this work, (D) (left axis) measured P_{NO}, (right axis) measured P_{pitot} (magenta). Probe 1 is shown in red and probe 2 is shown in black. Predictions from CFD using Park rates (dashed black) and Streicher rates (dashed blue). The vertical green lines indicate the quasi-steady test time. The data is for a low-enthalpy test.

The vibrational temperature initially starts out quite scattered, due to relatively low signal levels, and then tightens rapidly to a near-steady value. During the measurement time the vibrational temperature remains relatively flat and does not change substantially. At later times (>2000 μs) where the rotational temperature has dropped the vibrational temperature becomes increasingly noisy due to decreased hotband absorbance levels. The measured quasi-steady vibrational temperatures for probe 1 and probe 2 agree very well. From the CFD predictions there is not expected to be a significant difference (>10 K) in the vibrational temperature of NO between probe 1 and probe 2 and this is confirmed by the LAS measurements. The Streicher model predicts a substantially higher NO vibrational temperature as compared to the Park model. This could result from improved VT rates or an increased rate of VV transfer with N_2. It is not expected that flow disturbances will impact the vibrational temperature substantially due to the low pressures and short residence times (≈4 μs/cm).

The rotational temperature measurements initially come in below 150 K corresponding to the passage of the starting shock. It is reassuring to see that the first measurement for probe 1 agrees quite well with the first measurement for probe 2. This time should correspond to directly after the passage of the starting shock where boundary layers have yet to fully develop. The gas temperature then rises rapidly and plateaus for a short time. Around 800 μs the rotational temperature rapidly drops and reaches a quasi-steady value. For both probe 1 and probe 2 the rotational temperature seems to plateau and remain relatively constant between 1121 μs and 1691 μs. Later on in the test the rotational temperature drops in a quasi-linear fashion which may be indicative of driver gas contamination. Specifically, helium contamination is associated with a drop in the translational temperature, an increase in velocity, and a decrease in NO mass density [32]. The measured rotational temperature of probe 1 is consistently higher than that

Optics EXPRESS

measured by probe 2. This likely results from oblique shocks present on probe 1. Probe 2 has a consistently lower measured rotational temperature which is indicative of its lower disturbance of the flow. The agreement between CFD and the measured rotational temperature from probe 2 is phenomenal with the probe 2 measurements straddling the CFD predictions during the quasi-steady time. Lastly, the standard deviation of the measured rotational temperatures is low and only a few degrees indicating a high SNR and quasi-constant value.

The measured velocity is initially near 3250 m/s. Then the measured velocity drops in a quasi-quadratic fashion before reaching a quasi-steady value. The velocity appears to be relatively constant during the test time which is surprising given the fall in $T_{tr,rot}$, P_{NO}, and pitot pressure later in the test. The probe 2 velocity measurements are mostly within the standard error of the MTV measurements giving confidence in the accuracy of both measurements. The agreement of the probe 2 and MTV measurements with CFD predictions is superb during the quasi-steady test time. The probe 1 velocity measurements come in lower than the MTV and probe 2 measurements. This supports the hypothesis that probe 1 has introduced a non-negligible disturbance to the flow.

The measured NO partial pressure initially comes in around 5 Pa and then follows a trend similar to the rotational temperature. The P_{NO} measurements from probe 1 are substantially higher than those from probe 2. This is completely consistent with part of the gas having passed through an oblique shock for probe 1. This is because pressure has the largest relative change for air passing through an oblique shock and this is what is observed in the measurements. Lastly, the traces in P_{NO} and $T_{tr,rot}$ also seem to be highly correlated with the pitot pressure measurements. There is a slight delay in the pitot pressure measurements, which results from the pitot rake's placement further downstream in the test section.

5.2.2. LAS measurements at medium enthalpy

Figure S4 in the supplementary material shows time histories of LAS measured properties for a medium-enthalpy test using probe 2. It is not shown here due to its similarities with the low- and high-enthalpy tests. A high-level discussion of the results for the medium-enthalpy test is given here. The measured vibrational temperature is relatively constant and agrees best with the Park rate predictions. The rotational temperature follows a similar trend as the low-enthalpy case. After the quasi-steady time the rotational temperature drops rapidly and is around 8% lower than CFD predictions. The velocity follows a similar trend as the low-enthalpy case. After the quasi-steady period the velocity increases which is likely due to driver-gas contamination. The partial pressure of NO follows a similar trend as the rotational temperature and pitot pressure and comes in higher than CFD predictions. After the quasi-steady period P_{NO} decreases along with the rotational temperature and a subtle rise in velocity. Lastly, there does seem to be an oscillation in P_{NO} similar to that in the pitot pressure. The high measurement rate of the diagnostic was particularly important here so that these fluctuations could be resolved.

5.2.3. LAS measurements at high enthalpy

Figure 7 shows time histories for a high-enthalpy test using probe 2 (black). The other entities in the plot are discussed in section 5.2.1 for Fig. 6 and will not be repeated here. The quasi-steady test time appears to be between 486 μs and 694 μs. Table 1 tabulates the LAS measured properties and CFD predictions. The 95% CI bands in C and D are too small to be seen.

The vibrational temperature agrees best with the CFD predictions using Park rates. Compared to the low-enthalpy tests there seems to be more time-dependent variation in T_{vib}. After the quasi-steady test time, T_{vib} drops nearly 150 K to near 550 K. This later drop may be due to driver gas contamination lowering the vibrational relaxation time for all species (primarily resulting from helium contamination) thus making the gas vibrationally colder as a whole. However, this was not observed in the low-enthalpy test which may be due to differing gas conditions during the expansion. The rotational temperature follows a similar trend as the low-enthalpy case. However,

Optics EXPRESS

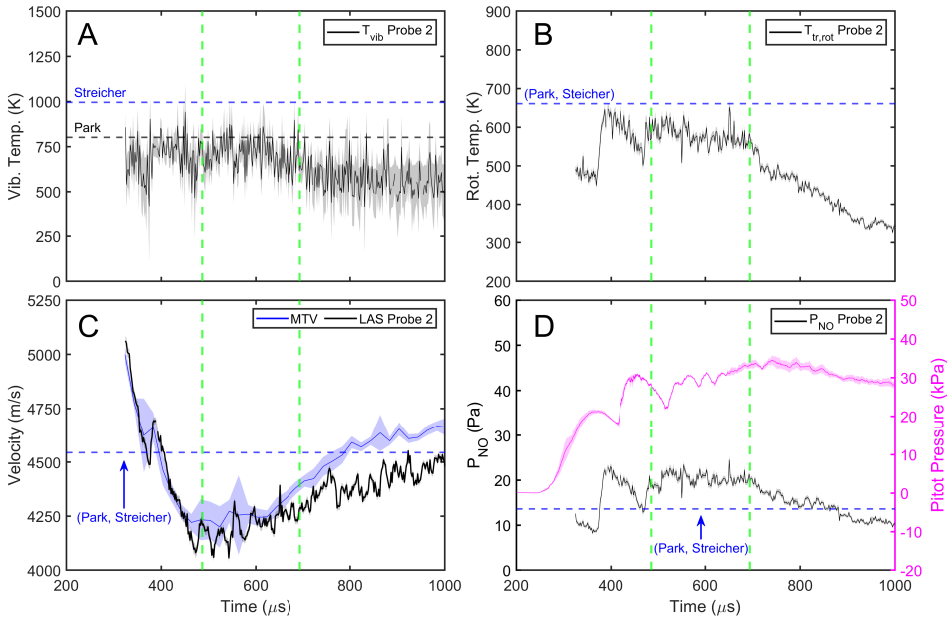

Fig. 7. (A) Measured T_{vib}, (B) $T_{tr,rot}$, (C) velocity by MTV (blue) [14] and probe 2, (D) (left axis) measured P_{NO}, (right axis) measured P_{pitot} (magenta). Predictions from CFD using Park rates (dashed black) and Streicher rates (dashed blue). The vertical green lines indicate the quasi-steady test time. Data is for a high-enthalpy test.

the initial peak does not seem to plateau for any noticeable time. The rotational temperature seems to rise rapidly and reach a quasi-steady value after the first drop. The rotational temperature measurements are lower than CFD predictions. In the velocity trace, after the initial drop and a short steady period, the velocity seems to increase in a linear fashion. The LAS measurements and MTV agree well with each other before and during the quasi-steady state and then diverge later. This may be related to how the MTV data is interpreted or non-uniform flow that arrives with driver gas contamination. Regardless, this later time is outside the intended operating regime of the facility. Both LAS and MTV velocities come in below the CFD predictions during the quasi-steady flow. Oscillations in the LAS velocity are observed and seem to correlate to increases in the standard error of the MTV measurements. The precision in the LAS velocity measurements is phenomenal and clearly shows velocity fluctuations in the flow. During the quasi-steady test time the oscillations have a frequency near 60 kHz and a peak-to-peak amplitude of nearly 140 m/s. The P_{NO} measurements have a similar trend to the low-enthalpy tests and the traces correlate well with $T_{tr,rot}$ and the pitot pressure measurements at early times. Later in the test the partial pressure of NO drops and seems to be quasi-linear with time and this is also observed in $T_{tr,rot}$. On the other hand, the pitot pressure seems to remain quasi-constant which could result from a combination of a decline in static pressure and a rise in velocity.

5.3. *Uncertainty analysis*

An analysis of the uncertainties in $T_{tr,rot}$, T_{vib}, and P_{NO} was performed in our previous work where the uncertainties from the 95% CI returned from the fitting routine and linestrengths were added in quadrature since they are the dominant sources of uncertainty [15]. The uncertainty in these quantities are expected to be the same here. The uncertainty in $T_{tr.rot}$, T_{vib}, and P_{NO} have maximum values of 2.1%, 3.9%, and 3.7%, across all test conditions, respectively. The uncertainty in the velocity was calculated by adding the uncertainty from the crossing angle and

Optics EXPRESS

the etalon characterization of frequency tuning in quadrature as these were the major sources of uncertainty in the velocity. Here, the uncertainty in the etalon characterization was determined by comparing the measured spacing of the transitions with that from the HITEMP2019 database [33,34] since the transitions linecenters are known with high accuracy. The total uncertainty in the measured velocity is estimated to be 1.53% and 1.55% for probe 1 and probe 2, respectively.

6. Conclusion

This manuscript presents the development and application of a QCLAS diagnostic capable of measuring the rotational and vibrational temperatures, partial pressure, and velocity of NO at 100 kHz or 500 kHz in hypersonic air flows with NO. Two different probe designs were tested in a hypersonic shock tunnel. Both probes utilized a retroreflected beam to provide self-referenced calibration-free velocity measurements using a single beam and detector. Comparison of LAS measurements from both probes are presented for low-enthalpy tests. The rotational temperature and P_{NO} measured by probe 1 were significantly higher than measurements using probe 2. This resulted from the mildly intrusive nature of probe 1, although, it should be noted that the probe 1 design was similar to those applied previously by other researchers [4,5,16,17]. The probe 2 measurements of the rotational temperature, NO partial pressure, and velocity agreed extremely well with CFD predictions for the low-enthalpy test. However, disagreement of the aforementioned properties with CFD was observed for medium- and high-enthalpy tests with the disagreement increasing with flow enthalpy. Two different sets of rates for NO vibrational relaxation were used in the CFD simulations in this work. The Streicher rates predicted the vibrational temperature of NO best at low enthalpy and the Park rates performed best at medium and high enthalpy. During the test time, transients primarily in the rotational temperature, NO partial pressure, and velocity were observed. The transient nature of the tests increased with increasing velocity. Pitot stagnation pressures were also presented and correlated well with the rotational temperature and NO partial pressure.

Funding. Laboratory Directed Research and Development program at Sandia National Laboratories.

Acknowledgment. This work was supported by the Laboratory Directed Research and Development program at Sandia National Laboratories. This paper describes objective technical results and analysis. Any subjective views or opinions that might be expressed in the paper do not necessarily represent the views of the U.S. Department of Energy or the United States Government. Sandia National Laboratories is a multimission laboratory managed and operated by National Technology & Engineering Solutions of Sandia, LLC, a wholly owned subsidiary of Honeywell International Inc., for the U.S. Department of Energy's National Nuclear Security Administration under contract DE-NA0003525.

Disclosures. The authors declare no conflicts of interest.

Data availability. The data for the results in this paper may be obtained upon reasonable request.

Supplemental document. See Supplement 1 for supporting content.

References

1. S. Gu and H. Olivier, "Capabilities and Limitations of Existing Hypersonic Facilities," Prog. Aeronaut. Sci. **113**, 100607 (2020).
2. J. Simmons, "Measurement Techniques in High-Enthalpy Hypersonic Facilities," Exp. Therm. Fluid Sci. **10**(4), 454–469 (1995).
3. I. Nompelis, G. V. Candler, and M. S. Holden, "Effect of Vibrational Nonequilibrium on Hypersonic Double-Cone Experiments," AIAA J. **41**(11), 2162–2169 (2003).
4. S. Wehe, D. Baer, R. Hanson, *et al.*, "Tunable Diode-Laser Absorption Measurements of Temperature, Velocity, and H_2O in Hypervelocity Flows," in *33rd Joint Propulsion Conference and Exhibit*, (1997), p. 3267.
5. S. Wehe, D. Baer, R. Hanson, *et al.*, "Measurements of Gas Temperature and Velocity in Hypervelocity Flows Using Diode-Laser Sensors," in *20th AIAA Advanced Measurement and Ground Testing Technology Conference*, (1998), p. 2699.
6. A. Mohamed, D. Henry, J. Faléni, *et al.*, "Infrared Diode Laser Absorption Spectroscopy Measurements in the SAMA, F4 and HEG Hypersonic Flows," in *International Symposium on Atmospheric Reentry Vehicles and Systems*, (1999).
7. R. Parker, T. Wakeman, M. Holden, *et al.*, "Measuring Nitric Oxide Freestream Concentration Using Quantum Cascade Lasers at CUBRC," in *44th AIAA Aerospace Sciences Meeting and Exhibit*, (2006).

Optics EXPRESS

8. R. Parker, T. Wakeman, M. MacLean, *et al.*, "Measuring Nitric Oxide Freestream Velocity Using Quantum Cascade Lasers at CUBRC," in *45th AIAA Aerospace Sciences Meeting and Exhibit*, (2007).
9. J. Meyers, S. Paris, and D. Fletcher, "Characterization of CO_2 Flow in a Hypersonic impulse Facility Using DLAS," Exp. Fluids **57**(2), 25 (2016).
10. J. J. Girard, P. M. Finch, C. L. Strand, *et al.*, "Measurements of Reflected Shock Tunnel Freestream Nitric Oxide Temperatures and Partial Pressure," AIAA J. **59**(12), 5266–5275 (2021).
11. P. M. Finch, J. J. Girard, T. Schwartz, *et al.*, "Measurements of T5 Shock Tunnel Freestream Temperature, Velocity, and Composition," AIAA J. **61**(4), 1555–1578 (2023).
12. C. W. von Rosenberg, K. N. C. Bray, and N. H. Pratt, "Shock Tube Vibrational Relaxation Measurements: N2 Relaxation by H2O and the CO–N_2 V–V Rate," The J. Chem. Phys. **56**(7), 3230–3237 (1972).
13. P. M. Finch, J. J. Girard, T. Schwartz, *et al.*, "Shock-Layer Measurements in T5 Shock Tunnel Hypersonic Flows Around a Cylinder Model," AIAA Journal pp. 1–24 (2024).
14. E. R. Jans, K. P. Lynch, R. M. Wagnild, *et al.*, "Laser Measurements and Modeling of Shock Tunnel Freestream Velocity and Multispecies Thermal Nonequilibrium," AIAA Journal (2025).
15. J. J. Gilvey, E. R. Jans, K. A. Daniel, *et al.*, "High-Speed Laser-Absorption Measurements of Non-Equilibrium Nitric Oxide in the Sandia Hypersonic Shock Tunnel," Appl. Phys. B **130**(11), 203 (2024).
16. R. Vallon, J. Soutadé, J.-L. Vérant, *et al.*, "A Compact Tunable Diode Laser Absorption Spectrometer to Monitor CO_2 at 2.7 μm Wavelength in Hypersonic Flows," Sensors **10**(6), 6081–6091 (2010).
17. Z. Xu, R. Kan, J. Ran, *et al.*, "A Tunable Diode Laser Absorption Based Velocity Sensor for Local Field in Hypersonic Flows," in *Optics and Photonics for Energy and the Environment*, (Optica Publishing Group, 2016).
18. T. Schwartz, P. M. Finch, C. L. Strand, *et al.*, "Laser Absorption Sensor Targeting Potassium for Hypersonic Velocity, Temperature, and Enthalpy Measurements," AIAA J. **61**(8), 3287–3297 (2023).
19. T. Schwartz, J. P. Santos, C. L. Strand, *et al.*, "Laser-Based In-Situ Absorption Spectroscopy Sensor for Gas Measurements in an Impulse Facility," in *AIAA SciTech 2023 Forum*, (2023), p. 2519.
20. D. Yun, S. C. Egbert, A. T. Frymire, *et al.*, "Single-Beam Velocimetry with Dual Frequency Comb Absorption Spectroscopy," Opt. Express **32**(11), 18650–18663 (2024).
21. J. Kurtz, M. Aizengendler, Y. Krishna, *et al.*, "Rugged, Scramjet Inlet Temperature and Velocity Sensor: Design and Ground Test," AIAA J. **54**(2), 399–407 (2016).
22. J. Kurtz, M. Aizengendler, Y. Krishna, *et al.*, "Subsonic In-Flight Temperature and Pressure Measurements Using a Scramjet Inlet Flow Sensor," AIAA J. **54**(3), 1011–1017 (2016).
23. W. Demtröder, *Laser Spectroscopy 1: Basic Principles* (Springer, 2014).
24. J. D. Anderson, *Hypersonic and High-Temperature Gas Dynamics* (American Institute of Aeronautics and Astronautics, 2019), 3rd ed.
25. K. P. Lynch, T. Grasser, R. Spillers, *et al.*, "Design and Characterization of the Sandia Free-Piston Reflected Shock Tunnel," Shock. Waves **33**(4), 299–314 (2023).
26. A. P. Nair, N. Q. Minesi, C. Jelloian, *et al.*, "Extended Tuning of Distributed-Feedback Lasers in a Bias-Tee Circuit via Waveform Optimization for MHz-Rate Absorption Spectroscopy," Meas. Sci. Technol. **33**(10), 105104 (2022).
27. C. Park, "Review of Chemical-Kinetic Problems of Future NASA Missions. I-Earth Entries," J. Thermophys. Heat Transfer **7**(3), 385–398 (1993).
28. M. K. Kim, B. Esser, U. Koch, *et al.*, "Numerical and Experimental Study of High Enthalpy Flows in a Hypersonic Plasma Wind Tunnel: L3K," in *42nd AIAA Thermophysics Conference*, (2011), p. 3777.
29. J. W. Streicher, A. Krish, and R. K. Hanson, "High-Temperature Vibrational Relaxation and Decomposition of Shock-Heated Nitric Oxide. I. Argon Dilution from 2200 to 8700 K," Phys. Fluids **34**(11), 116122 (2022).
30. J. W. Streicher, A. Krish, and R. K. Hanson, "High-Temperature Vibrational Relaxation and Decomposition of Shock-Heated Nitric Oxide: II. Nitrogen Dilution from 1900 to 8200 K," Phys. Fluids **34**(11), 116123 (2022).
31. S. P. Kearney, E. R. Jans, J. L. Wagner, *et al.*, "High-Speed Diagnostic and Simulation Capabilities for Reacting Hypersonic Reentry Flows (LDRD Final Report)," Tech. rep., Sandia National Lab.(SNL-NM), Albuquerque, NM (United States) (2022).
32. T. Gross and T. E. Schwartzentruber, "Freestream Characterization of Hypersonic Wind Tunnels by Combining Measurements and Simulation," in *AIAA Scitech 2023 Forum*, (2023), p. 2090.
33. L. S. Rothman, I. E. Gordon, R. J. Barber, *et al.*, "HITEMP, the High-Temperature Molecular Spectroscopic Database," J. Quant. Spectrosc. Radiat. Transf. **111**(15), 2139–2150 (2010).
34. R. J. Hargreaves, I. E. Gordon, L. S. Rothman, *et al.*, "Spectroscopic Line Parameters of NO, NO_2, and N_2O for the HITEMP Database," J. Quant. Spectrosc. Radiat. Transf. **232**, 35–53 (2019).